ANDERSON LOCALISATION AND DECOHERENCE

CID: 00944784

Supervisor: Florian Mintert

Assessor: Alejandro Valido

Project code: QOLS-MINTERT-2

Word count: 9017

Imperial College London

1 Joint declaration of work undertaken

Previous work was completed as part of summer UROP placement undertaken by CID: 00944784 and this project is an extension of that work.

CID: 00944784 investigated and verified the use of decoherence and averaging processes. Florian Mintert conceived the idea of using a tilted Hamiltonian with averaging methods to obtain a decoherence process. CID: 00944784 investigated the behaviour of localised states subject to the decoherence process and Yannic Rath provided details of prominent peaks using the master equation approach.

2 Abstract

The behaviour of Anderson localised eigenstates is studied in the presence of decoherence. A decoherence model is presented that consists of introducing a tilt term $\sum_k \alpha k|k\rangle\langle k|$, which shifts the energy levels across the system, and a statistical averaging over the variable α. The decoherence model is analysed analytically, whose predictions are then verified numerically. It is found through numerical work that that the model represents a decoherence process. A typical Anderson eigenstate is studied under the decoherence process and its secondary structures are analysed. It is found that the ratio R_p of the main peak's prominence to the secondary peak is $R_p = 0.17 \pm 0.01$ A prominent peak found using a different decoherence model is analysed numerically using the model presented here. In this case the ratio $R_p = 4.4 \pm 0.1$, meaning the secondary peak is larger than the initial main peak. The physicality of the model is discussed critically, in particular that while the addition of the tilt term has a solid physical interpretation, elements of the averaging process are less obvious.

3 Introduction

3.1 Anderson localisation

Since the pioneering work of P. W. Anderson [1], Anderson localisation has been an active field of research. Anderson localisation entails suppression of wave transport and exponential decay of the wave function away from a point [2], as shown in figure 1. Initially considered in disordered solids, AL has been studied and observed in a number of different settings: acoustic waves [3], light waves [4,5], microwaves [6], Bose-Einstein condensates (as matter waves) [7] and photonic lattices [8].

The classical model of conductivity in solids is the Drude model: electrons, considered free

particles, scatter off relatively immobile heavy ions according to an average distance between collisions, the mean free path l [9]. In solids however, l was found to be far larger than the lattice constant. Bloch waves, a quantum description of electrons in solids, remedy this problem. Due to the translational symmetry of the solid's crystals, the crystal momentum of the electron is conserved, and the Bloch wave travels through the solid at constant group velocity [10]. When the wave encounters an impurity in the lattice it is scattered, since the symmetry is broken. This explains the larger than expected mean free path in solids and also why the Drude model works well in predicting classical transport, e.g. Ohm's law [9]. Electrons do not scatter off ions, they scatter off *impurities* [10].

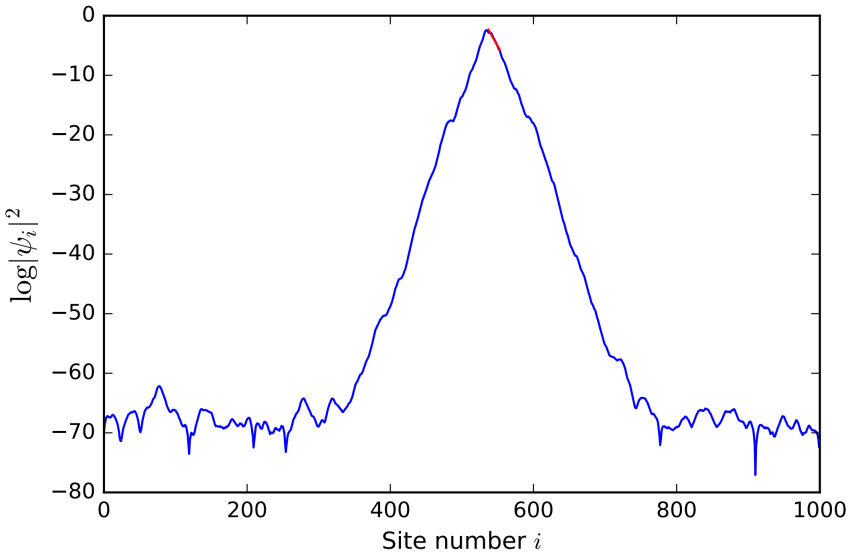

Figure 1: Plot of $\log|\psi_i^2|$ vs site number i. This shows the logarithm of the probability of finding a particle at site number i in the system. Notice that on the logarithmic scale the peak decays linearly from the site of the summit, this shows that the decay is exponential which is characteristic of Anderson localisation. Away from the peak computational noise is visible due to the logarithmic scale.

When the number of impurities, or amount of disorder, is sufficiently large this scattering via impurities results in Anderson localisation [11]. A typical localised eigenstate is shown in figure 1. Anderson localisation arises due to the interference of the many scattering paths with random path lengths and therefore random phases [12]. This results in destructive interference. This destructive interference results in the suppression of transport and exponential decay of the wave function away from a site in the system i.e. Anderson localisation. Since Anderson localisation relies on these interferences, it is logical to study Anderson localisation when the system is dephased, i.e. subject to decoherence. It is expected that the

localisation will be destroyed since there will be no interference, as the coherence length L_ϕ will be small.

To understand how Anderson localisation may occur, it is instructive to study weak localisation. Weak localisation, as the name suggests, occurs at a weaker disorder than Anderson localisation [13]. In the path integral formulation of quantum mechanics, an amplitude is calculated by summing all possible trajectories, or paths [14]. Consider the paths of a wave from point A to point B as in figure 2a. The paths, after leaving A, scatter from impurities randomly, and arrive at point B having taken distinct routes of different lengths. It follows that when *all* the possible paths are summed, because the path length and phase of a given path is random at point B, the amplitude from A to B averages to zero in the sum. Now consider figure 2b - a closed loop. There are two paths around the loop, which interfere constructively, so the amplitude of a particle returning to A is enhanced by a factor of two [13,9]. This only holds in the large L_ϕ regime, otherwise probabilities rather than amplitudes would be considered, then interference is not possible. Weak localisation is also characteristic for being destroyed by very weak magnetic fields [11].

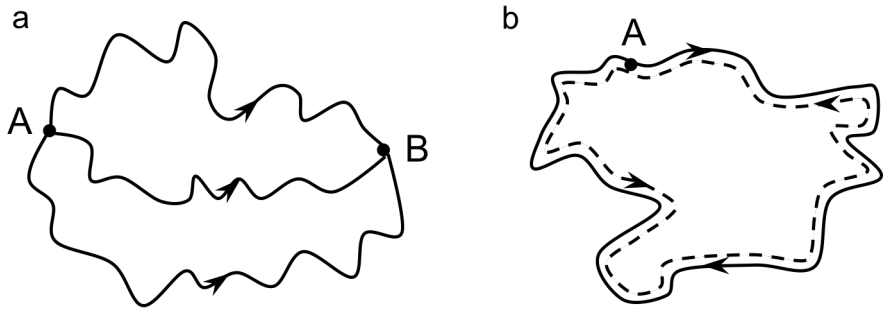

Figure 2: a) three possible scattering paths a particle could take from point A to point B. b) a possible path where the particle loops back on itself.

In the original paper by Anderson [1] he considered a lattice of n sites with energies ϵ_k. ϵ_k is taken to be random variable that has a probability distribution $P(\epsilon_k)$ parameterised by a width or strength of disorder W. The specific form of $P(\epsilon_k)$ is not important, usually it is a box distribution, however it can take other forms [2]. Particles are labelled by a site number j. Furthermore, there exists a hopping element between nearest neighbour sites t. The nature of t need not be specified, it can even be a random variable, however throughout we will take $t = 1$ [2]. The Hamiltonian H of the system can then be written

$$H = \sum_k \epsilon_k |k\rangle\langle k| + t \sum_k \left(|k\rangle\langle k+1| + |k+1\rangle\langle k| \right) \tag{1}$$

as in the paper [15]. In matrix form, the energies ϵ_k lie on the diagonal, with the hopping element t on the off-diagonals. We consider open boundary conditions, i.e a particle cannot hop from site n to site 1.

3.2 Decoherence

Decoherence is the process by which systems lose quantum coherence. A coherent quantum state is termed a pure state and can be defined in terms of the density matrix ρ as $Tr\rho^2 = 1$. The decoherence process transforms a pure state to a mixed state, for which $Tr\rho^2 < 1$ [16]. Quantum coherence is associated with adding *amplitudes* for events to happen, which allows interference, whereas in the classical case *probabilities* are added, which does not allow interference. Decoherence may then be viewed as a quantum to classical transition.

Physically, decoherence is induced by the interaction of the system with its environment, which suppresses interferences of the system very quickly [17]. Since Schroedinger evolution is unitary, i.e. it preserves coherence, decoherence processes must be modelled differently. A common route is to use a Lindblad master equation , which is the most general Markovian master equation that preserves the defining properties of ρ [18]. It reads

$$\dot{\rho} = -i[H, \rho] + \sum_i \gamma_i (L_i \rho L_i^\dagger - \frac{1}{2}\{L_i^\dagger L_i, \rho\}) \tag{2}$$

where the first term corresponds to unitary Schroedinger evolution and the second term represents the dissipative dynamics, the L_i are named Lindblad operators. For example, if the L_i are chosen to be projectors onto the eigenbasis of the system Hamiltonian H then the off diagonal elements of ρ, representing interferences, decay while the diagonal elements remain constant [19]. Note that it is defined $\hbar = 1$.

Intuitively, it is expected that as the decoherence is increased, the more classical the system becomes. It is important to note this picture does not always hold, as shown in a recent experiment involving multiparticle interference [20].

3.3 Previous work

We now summarise the previous work done on the dephasing of Anderson localised states. This work was based on the master equation formalism of equation 2. We start by making note of the useful Suzuki-Trotter expansion [22]

$$e^{\delta t(A+B)} = \lim_{\delta t \to 0} e^{A\delta t} e^{B\delta t} + O(\delta t^2). \tag{3}$$

Assuming that the solution of the dynamics induced by the Lindblad operators is of the form

$$\rho_{pq}(t) = e^{-\gamma|p-q|^2 t} \tag{4}$$

so that the off-diagonal elements of ρ decay exponentially whereas the diagonal elements are preserved as in the paper [19]. We then define the time-evolution operator $U(t)$ induced by the Hamiltonian H as $U(t) = e^{-iHt}$.

Then, using the Suzuki-Trotter expansion and equation 4 we may write the evolution of the density matrix elements as

$$\rho_{pq}(\Delta t) = e^{-\gamma_m (p-q)^2 \Delta t}(U(\Delta t)\rho U^\dagger(\Delta t))_{pq} + O(\Delta t^2) \tag{5}$$

where γ_m is a constant that controls the speed of the decoherence process. The system is evolved in N steps of Δt to evolve to time T, where $\Delta t = T/N$. To ensure this method is accurate, we minimise the error, so we have $\Delta t << 1$ or the number of steps $N >> 1$. Using this method Anderson localisation may be studied when subject to the decoherence process. We find the ground state of the original Anderson Hamiltonian, equation 1, by solving the eigenvalue problem numerically to find the eigenstates of the system. We may then pick out a particular eigenstate, usually the ground state, to study under the decoherence process of equation 5. See figure 3 for the evolution of a typical ground state of the Anderson Hamiltonian. The state, initially localised across $\sim$ 50 sites, spreads across the system with non-negligible probabilities for occupying many sites in the system. The off-diagonal elements of the density matrix decay exponentially and become negligible, meaning there is no quantum coherence and the system is classical.

As seen in figure 3, secondary structures, or secondary peaks peaks, appear in addition to the main peak. Relatively large probabilities accumulate for finding the particle at certain sites that have a large degree of independence from the initial peak. These secondary peaks were studied for a range of eigenstates. Peaks were labelled according to their prominence, which characterises the peak's independence. Specifically, we define the prominence of peak A as the vertical height of the peak above the *largest* minimum inbetween the peak and a larger peak B, conditional upon that there does not exist a peak C inbetween peak A and B larger than peak A. The process for finding the prominence of peak D is then: find the closest larger peaks, E to the left and peak F to the right. Choose the largest minimum inbetween peak E and F, then subtract the height of the minimum off the height of peak A. If there are no larger peaks then the prominence of the peak is just the peak's height. The degree to which these secondary peaks occurred was highly dependent on the specific eigenstate considered, i.e. with the same disorder strength W some peaks produced large

secondary peaks and others produced no appreciable peak e.g. the eigenstate considered in figure 2.

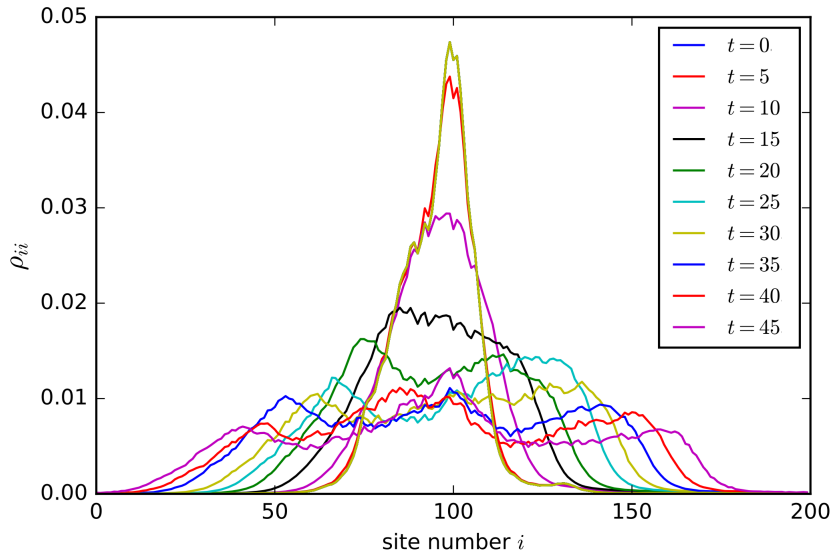

Figure 3: Plot of the diagonal elements of the density matrix ρ_{ii} vs the site number i. This represents the relative probability of finding a particle in different parts of the system as time evolves. We see that at $t = 0$ the system is in a localised eigenstate (the ground state of equation 1). A similar state is shown in figure 1. This means that particles are typically found in this area and are not free to propagate along the system. Since there is no transport at this time, there would also be zero conductance if this was a solid state system. As t increases the state spreads, becoming less localised and more classical as the decoherence process takes place. Of interest are the fine structures that appear for example the splitting of the peak into two structures at $t = 20$.

3.4 Aims and objectives

The exact nature of the transition between the non-classical Anderson localisation behaviour and the classical regime is unclear and has recently been the subject of some work [21,15]. The aim of the project is to analyse the decoherence process for Anderson localised eigenstates and particularly to analyse any secondary structures that emerge. Another central aim is to develop, verify and implement a decoherence process that is physically interpretable. This decoherence process will then be used to dephase Anderson localised eigenstates.

4 Methods

In previous work the method of simulating the dynamics relied upon the Lindblad master equation, equation 2. However, it is unclear how to implement such dynamics and there is no immediate physical interpretation. We seek a process with a more obvious interpretation that reproduces the results of the master equation approach.

We start from the Anderson Hamiltonian, equation 1, adding a term $\sum_k \alpha k|k\rangle\langle k|$that induces a tilt across the system

$$H = \sum_k \epsilon_k |k\rangle\langle k| + \sum_k \alpha k|k\rangle\langle k| + t\sum_k \left(|k\rangle\langle k+1| + |k+1\rangle\langle k|\right) \tag{6}$$

where α is an as yet unspecified constant. The effect of this extra term is to introduce a linear shift in energy levels across the system, where the shift is proportional to the site number. Therefore the effective shift between neighbouring sites is constant across the whole system. Intuitively, increasing the energy gap between neighbouring sites would be expected to reduce the quantum coherence of the system since a particle in the system requires more energy to tunnel to a neighbouring site.

First we consider the effect of the tilt term alone in the Hamiltonian. We then construct the time-evolution operator

$$U(t,\alpha) = e^{-i\sum_k \alpha k|k\rangle\langle k|t} = \sum_k e^{-i\alpha k t}|k\rangle\langle k| \tag{7}$$

where the second equality follows from Taylor expanding the first. We then consider the time evolution of a mixed state ρ, i.e. a state with off-diagonal density matrix elements

$$U(t,\alpha)\rho U^\dagger(t,\alpha) = \sum_{jk} e^{-i\alpha(k-j)t}|k\rangle\langle k|\rho|j\rangle\langle j| \tag{8}$$

we now consider the average of this quantity over an ensemble of different α so that

$$\langle U(t,\alpha)\rho U^\dagger(t,\alpha)\rangle_\alpha = \sum_{jk}\langle e^{-i\alpha(k-j)t}\rangle_\alpha |k\rangle\langle k|\rho|j\rangle\langle j| \tag{9}$$

now we assume that α is a random variable with a Gaussian distribution. We may then perform the averaging over α. Using the statistical result that the average of a quantity $A(x)$ that depends upon a random variable x with a probability distribution $P(x)$

$$\langle A(x)\rangle_x = \int dx P(x)A(x) \tag{10}$$

then, using that $P(\alpha) = \frac{1}{\sqrt{2\pi\sigma^2}}e^{-\alpha^2/2\sigma^2}$

$$\langle e^{-i\alpha(k-j)t}\rangle_\alpha = \frac{1}{\sqrt{2\pi\sigma^2}}\int d\alpha e^{-\alpha^2/2\sigma^2}e^{-i\alpha(k-j)t} \tag{11}$$

$$= \frac{1}{\sqrt{2\pi\sigma^2}}\int d\alpha\ e^{-\alpha^2/2\sigma^2 - i\alpha(k-j)t} \tag{12}$$

and by comparison with the standard Gaussian integral

$$\int_{-\infty}^{\infty} dx e^{-ax^2+bx+c} = \sqrt{\frac{\pi}{a}} e^{b^2/4a+c} \tag{13}$$

where in this case $a = 1/2\sigma^2$ and $b = -i(k-j)t$ so that

$$\langle U(t,\alpha)\rho U^\dagger(t,\alpha)\rangle_\alpha = \sum_{jk} e^{-(k-j)^2t^2\sigma^2/2}|k\rangle\langle k|\rho|j\rangle\langle j| \tag{14}$$

the elements of the density matrix ρ are Gaussian in distance from the diagonal element $(k-j)$. Furthermore they are Gaussian in time, rather than the expected exponential decay. If we discard this for a moment and assume we can perform the averaging in such a way as to obtain exponential decay in time, we may define a decay constant γ from equation 14

$$\gamma = \frac{(k-j)^2\sigma^2 t}{2} \tag{15}$$

then in this case we have a model of decoherence.

To understand this process of averaging and how we can make alterations to it, it is helpful to consider what is happening physically. For example, to simulate this system we would construct the time-evolution operator $U(t,\alpha_1)$, evolve the initial eigenstate (typically the Anderson localisation eigenstate shown in figure 1) to time δt. Then we would take another realisation of the time-evolution operator $U(t,\alpha_2)$ and evolve the eigenstate to time $2\delta t$, after N different realisations we would average over the result so that

$$\langle \underline{\underline{\rho}} \rangle_{\alpha_1 \ldots \alpha_N} = \frac{1}{N}\sum_{n=1}^{N} \underline{\underline{\rho}}_{\alpha_n} \tag{16}$$

where the double underline notation emphasises that we are now dealing explicitly with matrices so that the summation makes usage of matrix addition. Suppose we average over the ensemble using the method outlined and then take the density matrix $\langle \underline{\underline{\rho}} \rangle_{\alpha_1 \ldots \alpha_N}$, evolved to time δt, and repeat the process using $\langle \underline{\underline{\rho}} \rangle_{\alpha_1 \ldots \alpha_N}$ as the initial eigenstate. Say we repeat this process for a time τ, in m steps of time δt so that $\delta t = \tau/m$. The result is the expression

$$\langle U(\alpha,\delta t)\ldots\langle U(\alpha,\delta t)\rho U^\dagger(\alpha,\delta t)\rangle_\alpha \ldots U^\dagger(\alpha,\delta t)\rangle_\alpha \tag{17}$$

where we can substitute equation 14 m times to obtain

$$\langle U(\alpha,\delta t)\ldots\langle U(\alpha,\delta t)\rho U^\dagger(\alpha,\delta t)\rangle_\alpha \ldots U^\dagger(\alpha,\delta t)\rangle_\alpha = \sum_{jk} e^{-m(k-j)^2\delta t^2\sigma^2/2}|k\rangle\langle k|\rho|j\rangle\langle j| \tag{18}$$

where we can scale σ like $\bar{\sigma} = \sigma/\sqrt{m}$ so that this approach agrees with that of equation 14. This can also be seen as a convenient way to define σ such that the result does not depend

on the number of steps it was completed in. However, experimentally this would have to be built into the system beforehand changing σ depending on the value of m used. Now consider a different averaging technique where α is varied *before* the averaging is performed e.g

$$\langle U(\delta t, \alpha_m)...U(\delta t, \alpha_1)\rho U^\dagger(\delta t, \alpha_1)...U^\dagger(\delta t, \alpha_m)\rangle_{\alpha_1...\alpha_m} \tag{19}$$

in this case, for a specific realisation, the system is evolved with α_1 for time δt and then immediately evolved with α_2. Then the ensemble is averaged over using equation 16. In this case we can substitute equation 8, and then equation 7 repeatedly to obtain

$$\langle U(\delta t, \alpha_m)...U(\delta t, \alpha_1)\rho U^\dagger(\delta t, \alpha_1)...U^\dagger(\delta t, \alpha_m)\rangle_{\alpha_1...\alpha_m} = \sum_{jk} e^{-\frac{m(k-j)^2\sigma^2\delta t^2}{2}} |k\rangle\langle k|\rho|j\rangle\langle j| \tag{20}$$

we note here again that the m dependence may be removed by taking $\sigma \to \sigma/\sqrt{m}$ when constructing the time-evolution operator. Then, this approach yields the same result as equation 14. Noting that all methods of averaging over different realisations of the time-evolution operator so far have resulted in decay in time, now we will try to achieve exponential decay in time. If we evolve the system state, represented by ρ, for time δt using any of the above methods that results in Gaussian decay. We can then take the result $\rho(\delta t)$ and apply the same process resulting in further Gaussian decay for time δt. If we continue in this manner, at each step the density matrix ρ decays by the same amount which compounds into exponential decay. In terms of the time evolution operator this is represented by

$$\langle\langle U(\delta t, \alpha_m)...U(\delta t, \alpha_1)\rho(\delta t(a-1))U^\dagger(\delta t, \alpha_1)...U^\dagger(\delta t, \alpha_m)\rangle_{\alpha_1...\alpha_m} \tag{21}$$

where a is the number of steps the averaging is performed in and $\rho(\delta t(a-1)) = f(\delta t(a-1))$. Specifically

$$\rho(\delta t(b)) = \langle\langle U(\delta t, \alpha_m)...U(\delta t, \alpha_1)\rho(\delta t(b-1))U^\dagger(\delta t, \alpha_1)...U^\dagger(\delta t, \alpha_m)\rangle_{\alpha_1...\alpha_m} \tag{22}$$

where b is any natural number. So now equation 21 may be unpacked through substitution of equation 22 back to the initial step, where $b = 0$. It is hoped that computational simulations of this process will produce exponential decay of the off-diagonal elements of the density matrix ρ and therefore offer a more physical basis for a decoherence model of Anderson localisation.

Since the system Hamiltonian contains many random numbers, working with the Hamiltonian analytically is difficult. For example, when considering the evolution of the Anderson localisation under the decoherence process computational methods are required. The computational language used for the work was Python. Due to the nature of Hamiltonian (equation 1) in matrix form, i.e. a n by n matrix with a diagonal strip, it was essential to treat the

matrices as sparse and use the sparse matrix infrastructure where possible. This was particularly important to avoid memory errors and long run times as large n values were used. To obtain the eigenstates for the Anderson model, the eigenstates and eigenvectors needed to be found. So the problem is to find the ground state eigenvector as efficiently as possible, to allow larger system sizes to be used. The approach taken was to find only the eigenvector with the lowest energy, which is the ground state. To do this a function from the sparse linear algebra library was used. This function finds a few eigenstates around a specified energy E. To make this process efficient the specific Hamiltonian used, with $W = 0.1$ and $t = 1$, was studied to find the appropriate value of E such that it was close enough to the true ground state for the routine to be efficient but far enough away so that the first excited state was not chosen accidentally.

As the matrices dealt with become less sparse, for example when constructing the time-evolution operator of equation 7. The computational load becomes heavier. Some of the averaging processes, e.g that of equation 22, required producing and manipulating a large number of time-evolution operators $U(\alpha)$. In this case it was especially important to avoid loops that were not absolutely necessary and to experiment with ensemble sizes that ensured accuracy but also were time-economical. To study the model of equation 6 with added tilt term we would use the process from before to obtain an Anderson localised eigenstate. We would then make use of the sudden approximation, that concerns a sudden change in the Hamiltonian, it states that: if T is the time is takes for the Hamiltonian to change from H_1 to H_2, then in the limit $T \to 0$ the state of the system does not change [23]. In this case the time evolution operator is the identity, $U = 1$. We may derive a condition such that the sudden approximation holds. If we consider the Hamiltonian at time $t = cT$, then the initial Hamiltonian can be rewritten $H(c = 0)$ and the final Hamiltonian $H(c = 1)$. Consider the probability that the state ends up in a different state upon change of the Hamiltonian. This is given by the matrix element $\langle 0|U^\dagger(c)NU(c)|0\rangle$ where $|0\rangle$ is the initial ground state and $N = 1 - |0\rangle\langle 0|$, i.e. the projector onto vector space of vectors orthogonal to the ground state. Then we may perform perturbation theory on U the time-evolution operator for the change in H, to first order this reads

$$U(c) = 1 - iT \int_0^1 dc H(c)U(c) + O(T^2) \tag{23}$$

we define the quantity

$$\tilde{H} = \int_0^1 dc H(c) \tag{24}$$

substituting these two results into the matrix element yields the probability

$$\langle 0|U^\dagger(c)NU(c)|0\rangle = T^2\langle 0|\tilde{H}N\tilde{H}|0\rangle + O(T^3) \tag{25}$$

and substituting $N = 1 - |0\rangle\langle 0|$ we obtain (21:42)

$$\langle 0|\tilde{H}N\tilde{H}|0\rangle = \langle 0|\tilde{H}^2|0\rangle - \langle 0|\tilde{H}|0\rangle = (\Delta\tilde{H}^2) \tag{26}$$

where $\Delta\tilde{H}$ is the variance of the observable $\tilde{H}$ in state $|0\rangle$. Then we require this probability to be much less than one, because this would constitute the validity of the sudden approximation. The condition for validity of the sudden approximation is then that the time taken for the sudden change T is

$$T << 1/\Delta\tilde{H} \tag{27}$$

[23].

5 Results

When performing simulations, it was important to initially separate the terms of the Hamiltonian, equation 6. The idea is to make sure that the behaviour of the tilt term $\sum_j j\alpha|j\rangle\langle j|$ is understood first. That is, whether when various methods of averaging are performed, it behaves as expected before the other terms are introduced. This means that it would obey the simplest method of averaging shown in equation 14 and produce a Gaussian decay in time and distance from the diagonal of the density matrix. However, we are interested in the decoherence situation so we focus on the method defined by equations 21 and 22. Where the piecewise approach of varying α across a time period and then averaging over the ensemble of α at the end. This is repeated for the resulting density matrix and iterated through until the final step, which would be represented by time $a\delta t$ in the notation of equation 21. To verify the Gaussian decay was a column of the density matrix $|\rho_{1,i}|$ against the site number i and compared with the theoretically predicted plot. Figure 6 shows that is valid to plot one column of the density matrix as it is symmetric about the diagonal. We start by investigating simulations where the Hamiltonian contains only the tilt term. To simplify the problem further, we consider a starting state of $(\rho_0)_{pq} = 1$. To verify the process as deocoherence, exponential decay of the density matrix elements in time is required, with decay constant given by equation 15. Initially we consider the simplest averaging process, equation 14, and try to verify this result numerically. In this process the system is evolved using $U(t, \alpha)$ and then averaged over a large ensemble. Figure 4, where a column of the matrix is plotted in blue and equation 14 in green, shows that the elements of the density matrix decay in a Gaussian manner across the matrix. However, there are finite size effects as $n = 100$ sites, and the sample size of 400 realisations of α or $U(t, \alpha)$. Comparing figure 4 with figure 5, where the full column is visible and a much larger sample size of 10^4 is used, we see that the

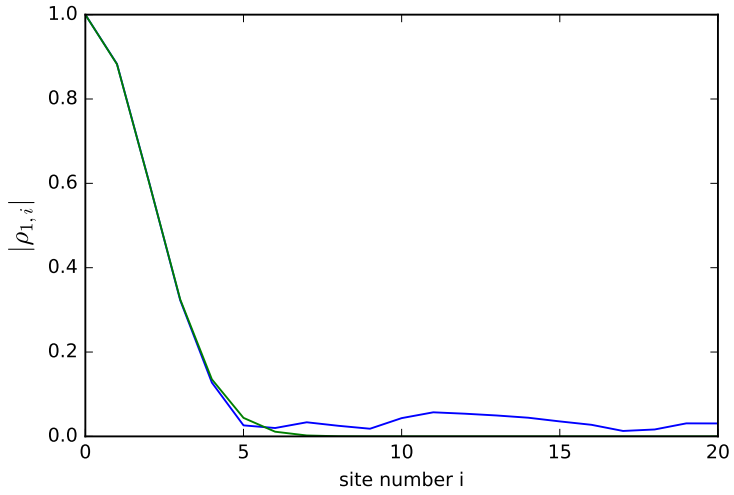

Figure 4: Plot of the elements of the first row of the density matrix $|\rho_{1,i}|$ (blue) against site number i after averaging over an ensemble of 400 α and of equation 14 (green). The standard deviation of the normal distribution governing α is $\sigma = 0.5$ and $(\rho_0)_{pq} = 1$. We see that the simulated plot has exactly the Gaussian shape up to approximately 5 sites with fluctuations seen past 5 sites.

fluctuations are almost eliminated. Specifically, the fluctuations are approximately 5 times smaller on average. Note that the system size was unchanged, so to reduce any fluctuations and improve accuracy it is effective to increase the sample size. This is important as there is a large memory cost associated with increasing the system size.

We now consider the more complicated averaging process defined in equations 21 and 22. To start, only the tilt term is considered. It is required that beforehand σ is corrected for m as outlined in the methods section. Figure 7 shows that the decay across the off-diagonal elements is indeed Gaussian, as expected. Again, the simulated line is shown in blue while the theoretical result is in green. Compared to the simpler process of figures 4 and 5, there are larger fluctuations. This is to be expected due to the more complicated nature of the process, which forces smaller ensembles sizes in order to maintain reasonable running times. Having verified the Gaussian decay in distance from the diagonal elements, consider now the decay in time. Figure 8 shows the result of applying the routine defined in equations 21 and 22 to the initial state $(\rho_0)_{pq} = 1$. The plot agrees well with small variations from the expected theoretical decay with constant $\gamma = \frac{(j-k)^2\sigma^2\delta t}{2}$. Figure 8 shows that this process does indeed decay exponentially in time, and furthermore with the decay constant γ. Therefore equations 21 and 22 represent a decoherence process. The average fluctuation of the data points from the theoretical values is a relatively small 10^{-3} when compared with the other figures. This

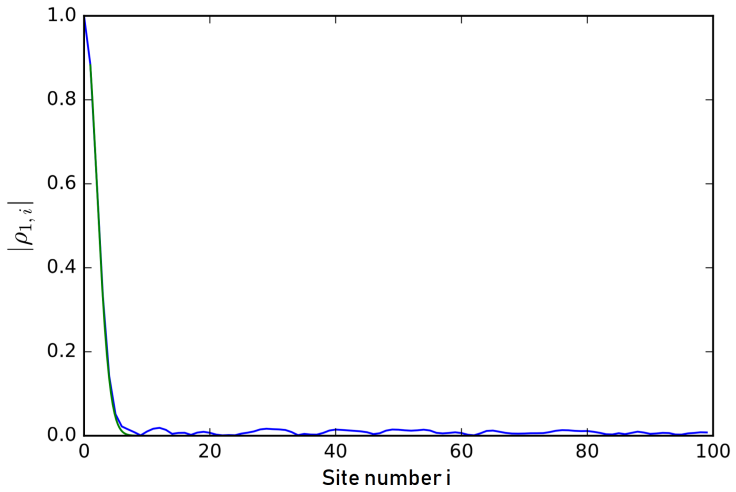

Figure 5: The same plot as in figure 3 but after averaging over an ensemble of 10^4 α. Note that the fluctuations are much smaller than in figure 1. Numerically, the average fluctuation was calculated to be approximately 5 times smaller than in figure 3.

is despite an unremarkable number of steps $m = 5$ and a relatively small ensemble size that is averaged over at each step. Compared to the $m = 6$ steps and 300 ensemble size of figure 8 that has an average fluctuation of 0.05, this is impressive accuracy. This can be thought of in terms of the process used to obtain an exponential decay. The Gaussian decay is taken advantage of by repeatedly compounding into an exponential decay. Each step, the system is only evolved for a small time so that it does not pass the point, e.g. after 5 sites in figure 4 and 7, where the fluctuations become larger. Although figures 4 and 7 are decays in site number i, the same rule applies for Gaussian decay in time.

Since it is verified that the process of equations 21 and 22 give Gaussian decay in distance from the diagonal element and exponential decay of the off diagonal elements in time, we now add in the next term: the hopping term $\sum_j t\Big(|j+1\rangle\langle j| + |j\rangle\langle j+1|\Big)$. At this stage we again consider the initial state as $(\rho_0)_{pq} = 1$. Then the time-evolution operator $U(t, \alpha)$ is constructed according to the process defined by equations 21 and 22.

As the hopping term is now present, this means it is possible for a particle to change site number. The propensity for a particle to do this depends upon the value of the hopping element t in relation to the strength of the disorder W and the standard deviation σ of the probability distribution of α. For example if $t/\sigma >> 1$ there is a large amount of hopping between sites. This means that the state spreads quicker across the system after the tilt is introduced. In figure 9, the width of the peak, a measure of spreading of the state, is plotted against the magnitude of the hopping element t. In the $t < \sigma$ regime, the spreading of the

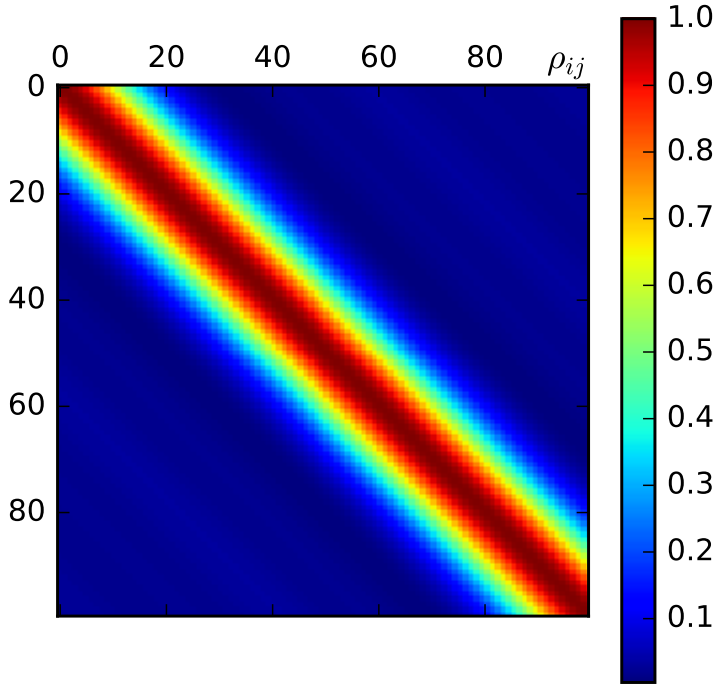

Figure 6: Plot of the elements of $(\rho_0)pq$, showing the symmetry along the diagonal, so we can choose any row of the density matrix to plot.

state is unaffected by increases in the magnitude of the hopping element t. However, when $t \approx 1.2$ increases in the hopping element t begin to produce greater spreading at the same time in the decoherence process. Past $t \approx 1.2$ the relationship between peak width and t is linear, which shows that the state spreads quicker across the system as you increase t. A corollary of this is that the diagonal elements ρ_{ii} may change in time. Contrast figure 10, where a column of the density matrix ρ is plotted against distance from the diagonal element with the hopping term included, with figures 7 and 8 where the Hamiltonian is just the tilt term with no hopping. The diagonal element is unchanged from the initial state $(\rho_0)_{pq} = 1$. In this case only the off-diagonal terms change, which shows there is no spreading of the state across the system. Furthermore, the decay away from the diagonal is still Gaussian, with the standard deviation given the same as the theoretical expression derived in equation 20 that considered a Hamiltonian with the tilt term alone. Similarly figure 11, where an element of the density matrix ρ is plotted against time, shows that the density matrix element decays exponentially in time from the initial value $(\rho_0)_{1,2} = 1$ with decay constant $\gamma = \frac{(j-k)^2\sigma^2\delta t}{2}$, where $\delta_t = 1$ in this case. Again we note the comparatively lower average fluctuation of 0.04 in this plot when compared with the Gaussian decay plot of figure 10 that has an average fluctuation of 0.06. While overall the fluctuations are larger

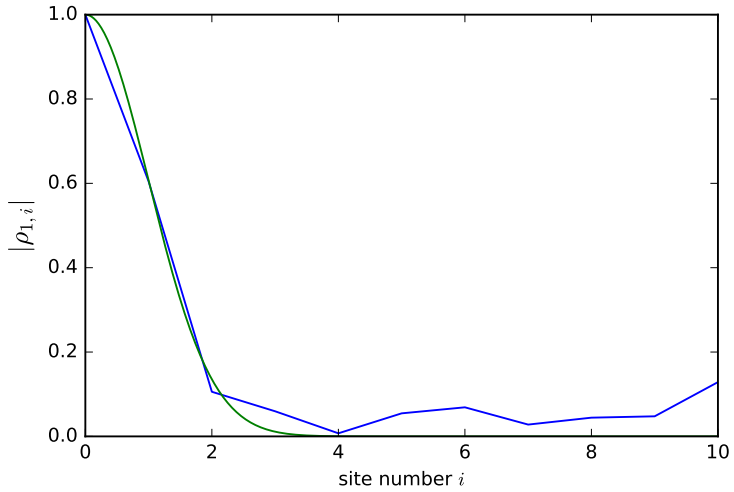

Figure 7: Plot of the first column of the density matrix $|\rho_{1,i}|$ against distance from the diagonal element or site number i. The Hamiltonian used has only the tilt term $\sum_j j\alpha|j\rangle\langle j|$. α, the random variable with a Gaussian distribution has $\sigma = 1$. α is varied in this case 6 times over the time interval, so $m = 6$. This is corrected for pre-emptively, thereby taking out the m dependence by taking $\sigma \to \sigma/m$. Then an averaging is performed over 300 realisations. The simulated plot, in blue, matches with the expected Gaussian shape shown in green of equation 20. Note that in this case, a smooth Gaussian is plotted, rather than that of figure 4 where the values of the Gaussian are plotted at the specific points where the domain exists, since the site number i is a natural number. The average fluctuation of the simulated plot points from the theoretical is 0.05 in this case.

than in the case with the tilt term alone, this may be attributed to the requirement of abandoning the sparse matrix infrastructure when constructing the time-evolution operator $U(t, \alpha)$. Furthermore, the ratio of fluctuation between the Gaussian plot and the exponential plot is smaller. A possible reason for this may be that in the case where the tilt term is used alone in the Hamiltonian, the ensemble size for the Gaussian plot was 300, whereas in the hopping term case it was 1000. In the decay plot, the ensemble size averaged over in the tilt alone case was 20 and 70 in the case when hopping is included. In the tilted Hamiltonian case, the number of steps m that the piecewise evolution is completed in is larger than when the hopping term was introduced. In the Gaussian case, $m = 6$ and $m = 3$ for the tilt alone and tilt with hopping term cases respectively. In the exponential case, $m = 5$ and $m = 4$ for the tilt term alone and hopping term respectively. This increase in number of steps increases the accuracy of the simulation, as the piecewise evolution becomes more continuous as m increases. Furthermore, with the addition of the hopping term, the diagonal element on the

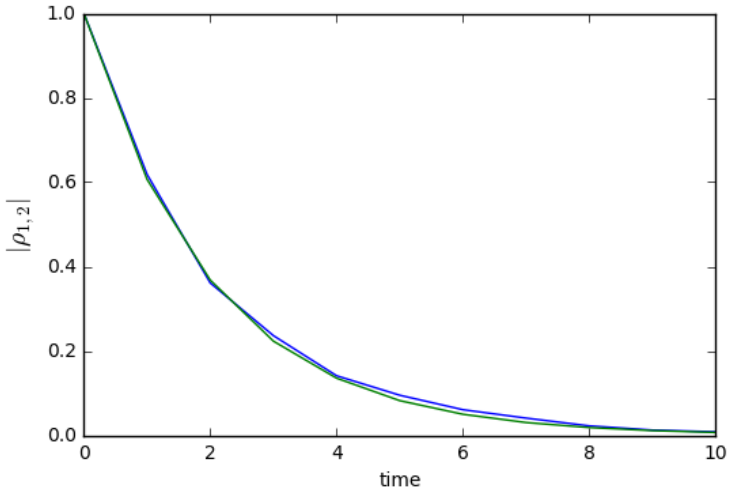

Figure 8: An element of the density matrix ρ is plotted against time. The Hamiltonian contains only the tilt term $\sum_j j\alpha|j\rangle\langle j|$. α was varied piecewise 5 times per time period. At the end of each time period an averaging over 20 piecewise realisations is performed. Plotted in blue is the simulation result and in green the expected exponential decay with decay constant $\gamma = \frac{(j-k)^2\sigma^2\delta t}{2}$. Interestingly, compared to figure 7, the average fluctuation of the plot points from their theoretical value is a much smaller 10^{-3}. In figures 4 and 7 we see clearly that as site number increases, the fluctuations increase. The same is true for Gaussian decay in time. Intuitively, the reason for this lower fluctuation is that in each step, the density matrix only experiences the initial accurate part of the Gaussian decay so the large inaccuracies are never introduced.

Gaussian plot are no longer equal to unity. The theoretically expected Gaussian is then compressed, which yields smaller fluctuations. A combination of the these factors are likely the cause of this difference in the ratio of the average fluctuations.

With both cases of the tilt term alone in the Hamiltonian and the tilt term including hopping established as following the theoretically expected results, we consider now the full model Hamiltonian, equation 6. With this step we add the disorder potential, $\sum_k \epsilon_k|k\rangle\langle k|$, where ϵ_k is a random number with a flat distribution so that $P(\epsilon_k) = 1/W$. As before, W is the disorder strength. Again, we use the initial state $(\rho_0)_{pq} = 1$ rather than an initial localised eigenstate, like that shown in figure 1. Figures 12 and 13 show that the theoretical predictions of Gaussian decay for distance from the diagonal element of the density matrix and exponential decay in time of the density matrix elements still hold, when the disorder potential was introduced. The fluctuations from the theoretical predictions are similar to the case with the Hamiltonian consisting of the tilt and hopping term. This is expected as

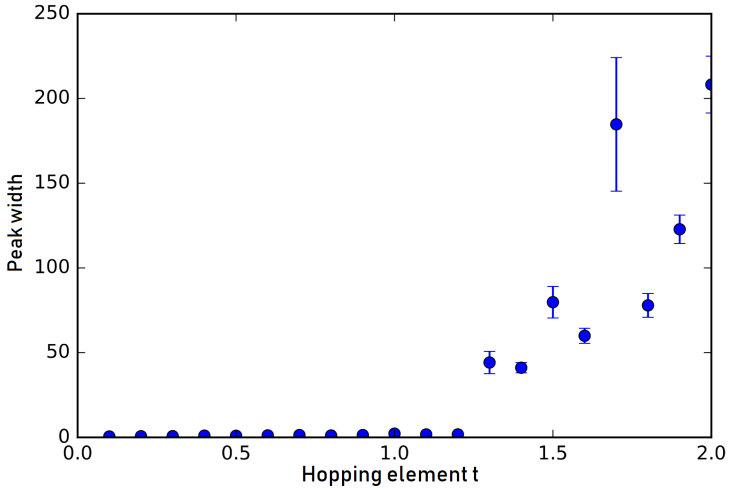

Figure 9: The width of the peak is plotted against the magnitude of hopping element t after $t = 6$ time units for a highly localised eigenstate using the decoherence process defined by equations 21 and 22. The standard deviation of the probability distribution governing $\sigma = 1$ in this case. It is necessary to use a localised eigenstate as the initial state ρ_0 in this situation to ensure there is a peak to analyse its spreading. It is hypothesised that as the hopping element increases, the system will spread quicker due to the enhanced likelihood of a particle hopping between sites. We observe that up to approximately 1.2 there is essentially no spreading in the system, after this there is a linear increase in the peak width which corresponds to a increase in spreading of the state. Each data point represents the averaging of 50 different realisations and the error bars represent 1 standard deviation of the distribution of peak width within the ensemble.

the ensemble sizes are identical in both cases for the Gaussian decay plots, $m = 1000$, and also for the exponential decay plots where $m = 70$. Furthermore, the number of steps that the piecewise evolution is completed in are equivalent in both the Gaussian and exponential decay cases. We have now established that the full model Hamiltonian, equation 6, can be used as a model for decoherence . There are important differences between this approach and the previous work where the master equation was used. In this case the decoherence behaviour follows naturally from the Hamiltonian, rather than having to be built in. Also, by using the Hamiltonian as a basis we allow an immediate physical interpretation, in terms of a localised system that is subject to a tilt.

Finally, we can consider the decoherence of the Anderson model in detail. It has been established that the process defined by equations 21 and 22 corresponds to a decoherence process, firstly with the tilt term alone, then with the hopping term added and finally with

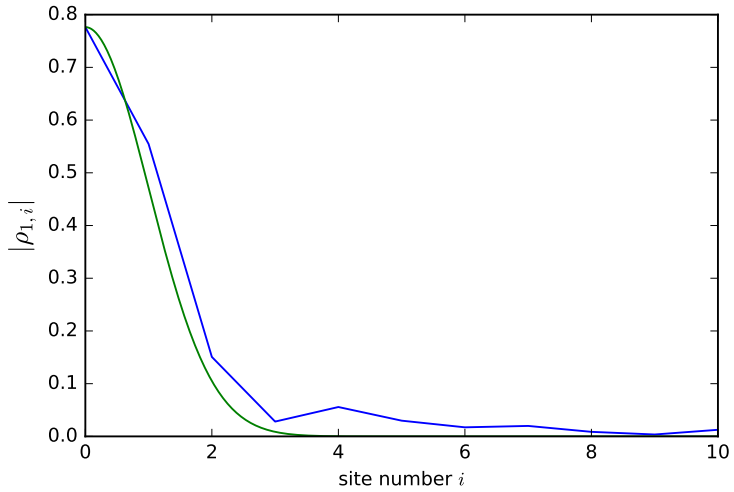

Figure 10: A column of the density matrix ρ plotted vs distance from the diagonal element. This is an analogous plot to figure 6. The initial state used is $(\rho_0)_{pq} = 1$ The Hamiltonian used has the tilt term $\sum_j j\alpha|j\rangle\langle j|$ plus the hopping term $\sum_j t\Big(|j{+}1\rangle\langle j|{+}|j\rangle\langle j{+}1|\Big)$. α, the random variable with Gaussian distribution of $\sigma = 1$, is varied in this case $m = 3$ times over the time interval. An averaging is performed over 1000 realisations. The simulated plot, in blue, matches with the expected Gaussian shape albeit with some noticeable deviation, similar to figure 7. The average fluctuation being 0.06, compared to 0.05 in figure 7. Although this plot uses a larger ensemble, 1000 compared to 300, which reduces the fluctuations, being unable to use the sparse matrix infrastructure when dealing with $U(t, \alpha)$ increases the magnitude of the fluctuations. This results in comparable accuracy between the plots. This plot differs from figure 7 in that the diagonal element differs from 1. This is due to the introduction of the hopping term, which means that the site may spread across the system and the diagonal elements ρ_{ii} are subject to change.

the disorder potential. Consider now an initial state that is localised, as in figure 1. We apply the decoherence process with the time-evolution operator $U(t, \alpha)$ containing the complete Hamiltonian. The decoherence process for a localised eigenstate is shown in figure 14, where the diagonal elements ρ_{ii} are plotted against site number. The process shown is representative of the evolution of an eigenstate using this method that is not selected specifically for the prominence of secondary structures. Similarly, an analogous plot using the master equation method is shown in figure 3. This is also chosen to be a typical representation of the average eigenstate using this method. In figure 13, the Anderson localised ground state has disorder strength $W = 1$. Then the piecewise evolution process is applied, with an identical procedure as before, i.e. that defined by equations 21 and 22, albeit with the initial eigenstate as an

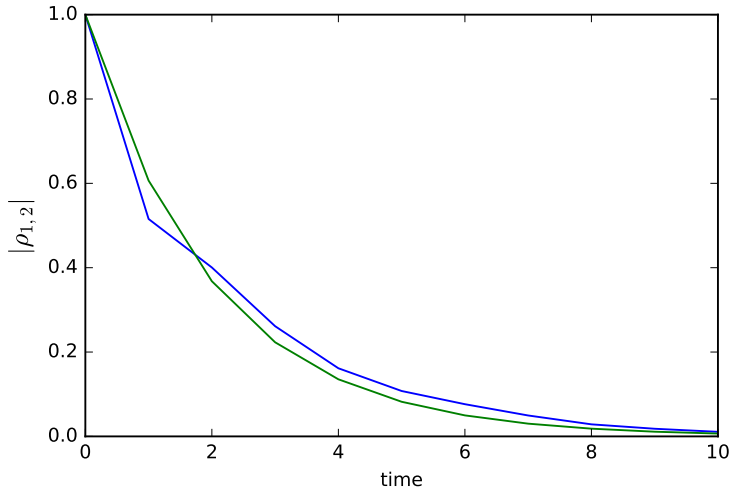

Figure 11: An element of the density matrix ρ is plotted vs time. The Hamiltonian has the tilt term $\sum_j j\alpha|j\rangle\langle j|$. α and the hopping term $\sum_j \mu\Big(|j+1\rangle\langle j| + |j\rangle\langle j+1|\Big)$. α was varied piecewise 4 times per time period T, so $m = 4$. At the end of each time period an averaging over 70 piecewise realisations is performed. Plotted in blue is the simulation result and in green the expected exponential decay with decay constant $\gamma = \frac{(j-k)^2\sigma^2\delta t}{2}$. The average deviation from the theoretically predicted exponential decay, shown in green, is 0.04.

Anderson localised ground state. In figure 14 the maximum secondary peak prominence occurs at t = 3, with a prominence of $P_s = 0.023 \pm 0.01$. Comparing this to the prominence of the main peak, $P_m = 0.13 \pm 0.01$, by taking the ratio $R = P_s/P_m = 0.17 \pm 0.01$. Note that even with an eigenstate not optimised for the maximum prominence of a secondary peak , the secondary peak prominence is still 17 percent of the main peak. Obtaining highly prominent secondary structures is highly dependent on the specific Anderson eigenstate chosen, i.e. its parameters W, t and more importantly the specific realisation of the eigenstate. In addition, the prominence depends on the standard deviation σ of the Gaussian distribution governing α. Due to the inherent randomness of the Anderson Hamiltonian, equation 1, in particular that every eigenstate has different structures. It then follows that the prominence of secondary structures varies considerably even when the same W, t and σ are used.

We now consider a localised eigenstate, and specific parameters, that have been chosen for the prominence of their secondary peaks when studied using the master equation approach, equation 5. The decoherence process is controlled by the parameter γ_m in this approach. It is important to write this parameter in terms of σ so that the decoherence process maximises the secondary prominences in our approach, as γ_m has been chosen to maximise secondary prominences in the master equation approach. We may obtain an expression for the standard

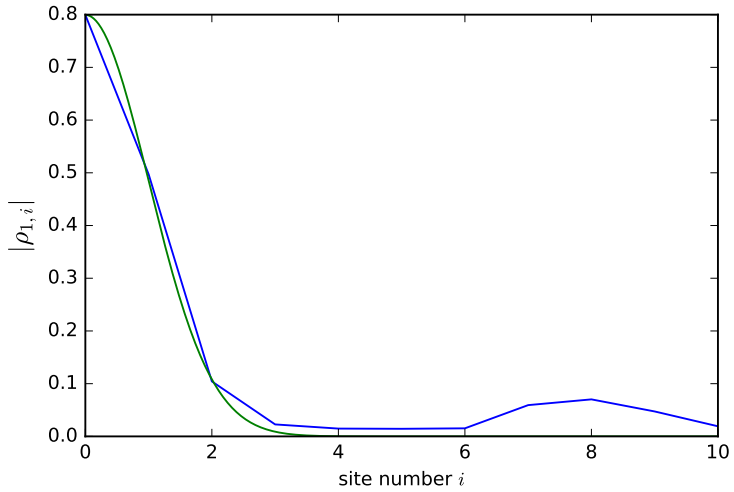

Figure 12: Column of the density matrix ρ plotted against distance from the diagonal element. The full model Hamiltonian with tilt term is used, equation 6. The random variable α with Gaussian distribution has $\sigma = 1$ and is varied in this case $m = 3$ times over the time interval. Then an averaging is performed over 1000 realisations. The simulated plot, in blue, matches with the expected Gaussian shape albeit with some noticeable deviation past site number $i = 6$. However, the average deviation between the theoretically predicted decay and the simulated result is 0.05. Compared to figure 10, which does not include the disorder potential term $\sum_k \epsilon_k |k\rangle\langle k|$ the average fluctuation is marginally larger, at 0.06.

deviation σ associated with α in terms of γ_m using equations 5 and 15

$$\gamma = \frac{(k-j)^2\sigma^2\delta t}{2} = (j-k)^2 = \gamma_m \tag{28}$$

then

$$\sigma = \sqrt{\frac{2\gamma}{m\delta t}}. \tag{29}$$

From this we compute the required σ. In the case of the localised state shown in figure 15, the required value is $\sigma = 0.001$. In the master equation approach, equation 5, the maximum prominence for the secondary peak of the localised state in figure 15 occurs at $t = 56$. We see from figure 15 that maxmimum prominence of the secondary peak occurs between $t = 50$ and $t = 60$. The specific value is $t = 57 \pm 1$, note that this value is rounded up to the nearest integer. The prominence P_s of the peak at this time is its height $P_s = 0.044 \pm 0.01$ and the ratio of the prominences is $R_p = P_s/P_m = 4.4 \pm 0.1$. In this instance, the t value corresponds to the time at which the peak is at its largest height and we note that the secondary peak is actually now the main peak, as can be seen at $t = 60$ in figure 15. This result is physically surprising because at $t = 0$ the state is localised in the region 10 sites either side of a

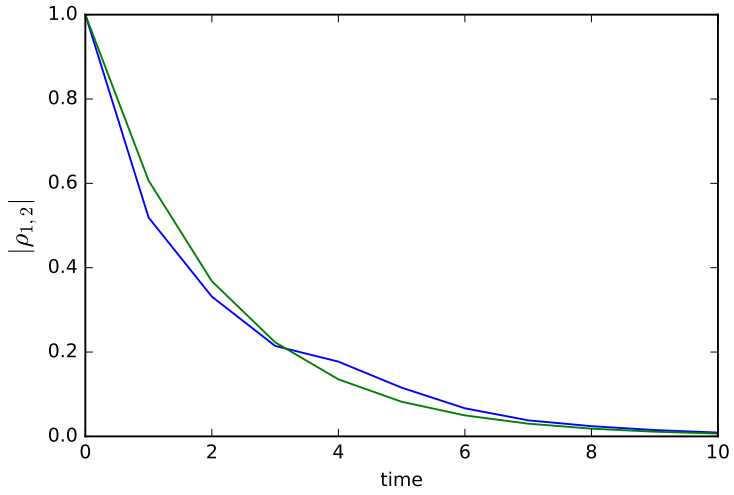

Figure 13: An element of the density matrix ρ is plotted vs time. The full Anderson Hamiltonian with tilt term is used. α was varied piecewise $m = 4$ times per time period. At the end of each time period an averaging over 70 piecewise realisations is performed. Plotted in blue is the simulation result and in green the expected exponential decay with decay constant $\gamma = \frac{(j-k)^2\sigma^2\delta t}{2}$. The average fluctuation in this case is 0.03, which is comparable to the 0.04 of figure 11.

strong peak in probability at site number 71. If a measurement of a particle's position in the lattice you would expect to find it at site number $i = 71 \pm 6$, where the uncertainty is derived from the RMS spread of the peak calculated using its statistical moments. Then at a point in the decoherence process a secondary peak, that is seemingly independent of the inital localised eigenstate, becomes more prominent than the main peak. Furthermore, past $t = 60$, the main peak's prominence eventually decreases further such that to a point disappears entirely and the only visible peak is the secondary peak.

6 Discussion

It has been shown in detail that the averaging process defined by equations 21 and 22 is a model for decoherence. The decoherence model was then used to examine the evolution of Anderson localised eigenstates. This process is an extension of the previous averaging processes, where it was found that by letting the constant α be a random variable with a Gaussian distribution resulted in a Gaussian decay of the density matrix elements in time. The decoherence process was then formed by combining the iterative averaging process of equation 18 and the piecewise averaging process of equation 19. An aim of the project was

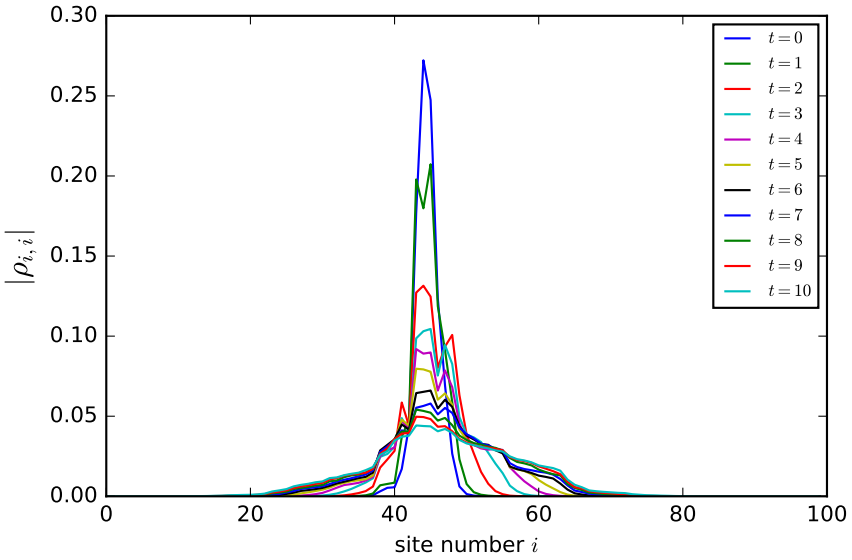

Figure 14: The diagonal elements of the density matrix ρ_{ii} are plotted against site number i. This plot is analogous to figure 2. This initial eigenstate is localised, with disorder strength $W = 1$. This figure shows a typical decoherence process for a localised eigenstate using this process. Here the maximum secondary peak prominence occurs at t = 3, with a prominence of $P_s = 0.023 \pm 0.01$. Comparing this to the prominence of the main peak, $P_m = 0.13 \pm 0.01$, by taking the ratio $R_p = P_s/P_m = 0.17 \pm 0.01$. Note that even though this state is not optimised for the maximum prominence of secondary peaks, the secondary peak prominence is 17 percent of the prominence of the main peak. Obtaining highly prominent secondary structure is highly dependent on the specific Anderson eigenstate chosen, i.e. its parameters W, t and most important the specific eigenstate's properties.

to obtain a more physically interpretable decoherence process than of that used in previous work. While the Hamiltonian can be readily interpreted physically, the averaging process is more complex. The piecewise process of equation 19 is easily understood: the state is evolved for time δt with the time-evolution operator $U(\delta t, \alpha_1)$ and then evolved for another δt for with time-evolution operator $U(\delta t, \alpha_2)$ etc. This is performed for a number of times and then the ensemble is averaged over using equation 16. The interpretation of the iterative average is less obvious. The state is evolved for time δt using $U(\delta t, \alpha)$ and is then averaged over an ensemble. The result is then taken and evolved for time δt. Then it is averaged over an ensemble. That the averaging is performed before the steps, rather than the end is the problem. It is difficult to imagine a physical system that replicates this as it would require the system to average over itself, and then use the result of the averaging. In the piecewise process, it would be possible to apply the time-evolution operator repeatedly and record the

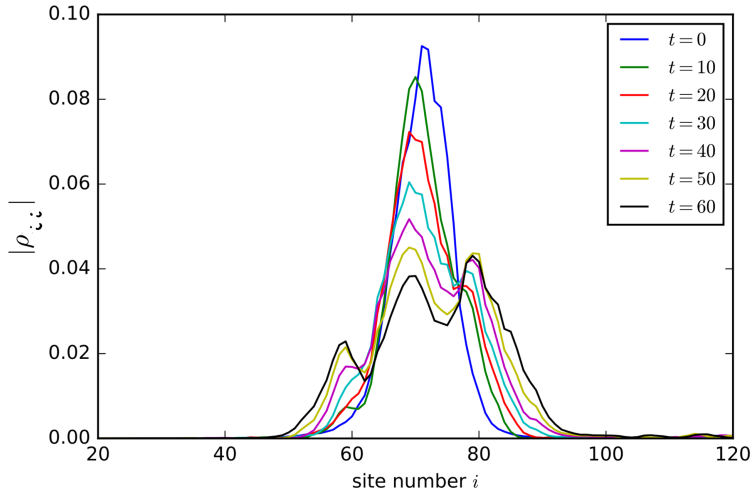

Figure 15: The diagonal elements of the density matrix ρ_{ii} are plotted against the site number i for a localised eigenstate selected for its prominent secondary peaks. The strength of disorder is $W = 1$ and the standard deviation of the distribution governing the random number α is $\sigma = 0.001$ Maximum secondary prominence occurs at $t = 57 \pm 1$, where the secondary peak's height is actually greater than the main peak. The prominence at this time is $P_s = 0.044 \pm 0.001$. The ratio of the prominences of the initial main peak P_m and initial secondary peak P_s is $R_p = 4.4 \pm 0.1$. The plot shows that at $t = 60$ the main peak is lower than the secondary peak. In addition, at larger times the main peak's prominence decreases to a point where it disappears entirely the secondary peak is only visible.

result. Then after repeating this process the averaging could be performed on the recorded results. A possible way around this would be to perform this kind of averaging, and then prepare the averaged state artificially.

As mentioned in the aims and objectives, the effect of decoherence on the Anderson model has been studied recently. It has been shown that introducing dissipation, via local dissipators as Lindblad operators within the master equation formalism, Anderson localition can be driven into a mixed steady state localisation which has tunable properties [21]. Furthermore, the author showed that in the regime of strong localisation, i.e. where the width of $P(\epsilon_k)$ is large, dissipation of this kind results in a robust delocalisation. This work is similar to the previous work, in that the master equation formalism is used and also comparable in that there is analysis of the resulting states after decoherence. However, it focuses on the resulting tunable localisation of steady states. Rather than on the dynamic secondary structures that appear and the evolution of the state under decoherence.

In the discrete one dimensional Anderson model of equation 1, the transition between Anderson localisation and classical ohmic behaviour has been solved analytically [15]. The

work confirms that, as expected, the classical relationship of the conductance G as a function of length L

$$G(L) = aL^{d-2}, \tag{30}$$

where a is a constant and d is the number of dimensions, holds even if there is disorder so long as an appropriate amount of decoherence is introduced. This is quantified by the condition for classical conductance that the coherence length L_ϕ must obey

$$L_\phi < \frac{1}{1 - \exp\left(-\zeta^{-1}\right)} \tag{31}$$

where ζ is a generalised second order Lyapunov exponent. Generalised Lyapunov exponents relate to the intermittency of a dynamical system, i.e. the jumping between periodic and chaotic motion [24]. This work is similar since it uses a statistical model for decoherence. It differs from this work since it focuses on examining analytically when the system starts to conduct in a classical manner. Furthermore, *weak* localisation has been considered in the context of decoherence [25].

When performing the simulation work, it was important to avoid computational precision errors. The numerical error in floating point number operations are approximately 10^{-15} [26]. With the accuracy typically given in the numerical results, one or two significant figures, the precision errors are negligible. Furthermore, when implementing the summation in equation 16, which commonly can cause large rounding errors. A routine that minimised the rounding error was chosen.

7 Conclusion

The aim of the project was to analyse the decoherence process for Anderson localised eigenstates and analyse any secondary structures that emerged as a result of the decoherence. Another central aim was to develop, verify and use a more physically interpretable model of the decoherence process. It was found that a combination of the model Hamiltonian equation 6 and the averaging process of equations 21 and 22 constituted a decoherence process. The model Hamiltonian was readily interpretable. But as mentioned in the discussion the decoherence process, while interpretable, would not be easy to implement experimentally. Further work could be done on the averaging process to make it more amenable to implementation. Then the new decoherence process would be verified, and the evolution of localised states analysed similarly. The decoherence process of Anderson localised eigenstates was analysed for a typical state with unremarkable secondary structures, and one that was optimised to maximise the prominence of secondary structures. This could be investigated further, to investigate exactly how incident these states with large secondary structures are.

8 Acknowledgements

I would like to acknowledge my supervisor Florian Mintert and Rob Nyman for their helpful guidance and patience.

9 Bibliography

[1] P. W. Anderson. Absence of diffusion in certain random lattices. *Phys. Rev.*, 109:1492, 1958.

[2] B. Kramer A. MacKinnon. Localisation: theory and experiment. *Rep. Prog. Phys*, 56:1469, 1993.

[3] R. L. Weaver. Anderson localisation of ultrasound. *Wave Motion*, 12:129, 1990

[4] D. S. Wiersma et al. Localisation of light in a disordered medium. *Nature*, 390:671,1997.

[5] M. Stoerzer et al. Observation of the critical regime near anderson localisation of light. *Phys. Rev. Lett.*, 96, 2009.

[6] A. A. Chabanov et al. Statistical signatures of photon localisation. *Nature*, 404:850, 2000.

[7] J. Billy et al. Direct observation of Anderson localization of matter waves in a controlled disorder. *Nature*, 453:891, 2013.

[8] T. Schwartz et al. Transport and anderson localization in disordered two-dimensional photonic lattices. *Nature*, 453:891, 2008.

[9] A. Lagendijk et al. Fifty years of anderson localisation. *Physics Today*, 62:24, 2009.

[10] U. Roessler. Solid state theory. Springer, 2009.

[11] B. L. Altshuler P. A. Lee. Disordered electronic systems. *Physics Today*, 41:36, 1988.

[12] P. E. Lindelof et al. New light on the scattering mechanisms in si inversion layers by weak localisation experiments. *Physica Scripta*, 1986.

[13] S. Datta. Electronic transport in mesoscopic systems. Cambridge University Press, 1995.

[14] R. P. Feynman. Space-time approach to non-relativistic quantum mechanics. *Rev. Mod.Phys*, 20:367, 1948.

[15] M. Zilly et al. Decoherence induced conductivity in the discrete 1d anderson model. *Phys. Rev. B*, 85, 2011.

[16] C. J. Isham. Lectures on quantum theory. Imperial College, 1995.

[17] M. Schlosshauer. Decoherence, the measurement problem, and interpretations of quantum mechanics. *Rev. Mod. Phys.*, 76:1267, 2005.

[18] H. P. Breuer et al. The theory of open quantum systems. Oxford, 2002.

[19] R. A. Bertlmann et al. Decoherence modes of entangled qubits with neutron inferometry. *Phys. Rev. A*, 73, 2006.
[20] R. Young-Sik et al. Nonmonotonic quantum-to-classical transition in multiparticle interference. *PNAS*, 110:1227, 2012.
[21] I. Yusipov et al. Localisation in open quantum systems.*Phys. Rev. Lett.*, 118, 2017.
[22] N. Hatano M. Suzuki. Quantum annealing and other optimisation methods. Springer, 2005.
[23] A. Messiah. Quantum mechanics. Dover books, 1961.
[24] G. Paladin A. Vulpiani. Anomalous scaling and generalized lyapunov exponents of the one-dimensional anderson model. *Phys. Rev. B*, 35:2015, 1986.
[25] D. S. Golubev, A. D. Zaikin. Quantum decoherence and weak localization at low temperatures. *Phys. Rev. B*, 51:9195, 1999.
[26] Python Software Foundation. Floating Point Arithmetic: Issues and Limitations. 2018, accessed through *docs.python.org/2/tutorial/floatingpoint.html*.